Rapid Communication

Monte Carlo simulation on dielectric relaxation and dipole cluster state in relaxor ferroelectrics*

Zhu Chen(朱 琛) and Liu Jun-Ming(刘俊明)†

Laboratory of Solid State Microstructures, Nanjing University, Nanjing 210093, *China*
International Center for Materials Physics, Chinese Academy of Sciences, Shenyang 110016, *China*

(Received 15 April 2010; revised manuscript received 20 April 2010)

The Ginzburg–Landau theory on ferroelectrics with random field induced by dipole defects is studied by using Monte Carlo simulation, in order to investigate the dipole configuration and the dielectric relaxation of relaxor ferroelectrics. With the increase of random field, the dipole configuration evolves from the long-range ferroelectric order into the coexistence of short-range dipole-clusters and less polarized matrix. The dipole-cluster phase above the transition temperature and superparaelectric fluctuations far below this temperature are identified for the relaxor ferroelectrics. We investigate the frequency dispersion and the time-domain spectrum of the dielectric relaxation, demonstrating the Vogel–Fulcher relationship and the multi-peaked time-domain distribution of the dielectric relaxation.

Keywords: relaxor ferroelectrics, domain structure, relaxation spectrum, Ginzburg–Landau theory

PACC: 7780, 7780D, 7740, 7780B

1. Introduction

Relaxor ferroelectrics (RFs) represent a specific class of ferroelectric (FE) materials whose dielectric and ferroelectric behaviours are unusual and different from normal ferroelectrics (NFs).[1−4] For example, RFs usually exhibit diffusive phase transitions and significant frequency dispersion in terms of dielectric susceptibility χ as a function of temperature T, while NFs offer a sharp transition peak and much weaker frequency dispersion. Furthermore, the excellent piezoelectric and electromechanical performances of RFs and high dielectric susceptibility are of special interest for sensor and transducer applications in smart structures,[5] although the physical mechanisms responsible for these superior properties have not yet been well understood so far.[6,7]

Intensive studies on RFs have collected a huge amount of knowledge on the relationships between the microstructure and property of RFs.[6−15] It is believed that most RFs are inhomogeneous in nanoscale and consist of nanosized more polarized regions coexisting with less polarized regions below a certain temperature (typically 10^2 K), whereas the more polarized and the less polarized regions may be viewed as FE phase (clusters) and paraelectric (PE) phase in a less strict sense respectively. Here it should be mentioned that for some RFs, the microstructure consists of FE clusters randomly embedded in the matrix of PE phase,[16−19] where spherical random bond random field model may hold ture.[9] However, the coexistence of more polarized regions and less polarized ones seems to be a more general scenario for RFs,[19] with a typical characteristic length comparable to the chemical short-range order.

Furthermore, it is well believed that the dipole clusters may even appear well above temperature $T_{\rm m}$ at which $\chi(T)$ reaches a maximum. This microstructure of two-phase existence plays an essential role in determining the dynamic response of χ of the whole system to external electric field E, and thus resulting in the frequency dispersion and diffusive ferroelectric transitions. The relatively easy relaxation dynamics of the dipole-clusters in RFs is argued to be responsible for the excellent electromechanical property and giant χ, considering the fact that NFs are facilitated with long-range dipole order and thus hard to respond to external fluctuations of E as $T << T_{\rm c}$.

Along this line, experimental and theoretical studies on the microstructures and dielectric physics of RFs in last several decades have been conducted. The-

*Project supported by the National Natural Science Foundation of China (Grant Nos. 50832002 and 10874035), and the National Basic Research Program of China (Grant No. 2009CB623303).
†Corresponding author. E-mail: liujm@nju.edu.cn
© 2010 Chinese Physical Society and IOP Publishing Ltd

oretically, a series of random field models including the compositional inhomogeneity model,[4] the micro–macro domain transition model,[4] the superparaelectric model,[7] the dipole–glass model,[9] the order–disorder model[6] and the random-bond-random-field model[2,9,20] were proposed in order to explain the experimentally observed effects for various RFs. While the random-bond-random-field model refers to two-phase coexistence in the mesoscopic scale, the other models emphasize more on the nanoscale features. Recently, the dipole defect model proposed by Semenovskaya and Khachaturyan[11] and Su *et al.*[15] has received much attention. It originates from the following experimental findings. As is well known, those RFs that have been well studied so far are doped perovskite oxides, such as A-site La-doped $Pb(Zr_xTi_{1-x})O_3$ (PLZT), B-site Mg-doped $PbNbO_3$ (PMN), B-site Zr(Hf)-doped $BaTiO_3$ etc., in which the doping is believed to introduce local dipole defects responsible for the abnormal behaviours of RFs.[2,10,12,20] These defects can be either impurity atoms distributed randomly in the lattice or off-centre dopant ions which generate internal random fields, or even a frustration of long-range ordering state due to some reasons.[2] In addition, the implantation of external particle beam such as electrons, protons and ions into NFs would be able to generate extrinsic defects so that the implanted NFs eventually evolve into RFs.[12] Therefore, the local polarization at these defect sites may be suppressed or enhanced, depending on the types of interaction between these defects and the lattice. The role of these defects is considered in the theoretical models in direct or indirect manners. For example, in the compositional inhomogeneity model, the defects may be impurity atoms or dopant ions.[4,9] For the former, the impurity atoms in the lattice are viewed as disordered (random) static defects coupled locally with the transformational mode which is responsible for a stable dipole. Therefore, the defects may reduce the magnitude of local dipoles from site to site. For the latter, if the lattice is doped by off-centre dopants, a local dipole will form and the local dopant may occupy one of the crystallographically equivalent off-centre sites around the unit cell centre, and the resultant dipole moment may align along one of the equivalent vectors. Such an off-centre displacement may lead to an enhancement of local dipole moment.

The microscopic mechanisms described above provide a physically sound basis for the dipole defect model. This model begins from the Ginzburg–Landau (GL) approach to NFs[21,22] although other models were also employed.[23–25] This model imposes the spatial random field by introducing random fluctuations in the Landau potential on the dipoles, which correspond to the randomly distributed dipole defects.[11,15,16] Thus, the dipole defect model is of microscopic sense, and represents a realistic description of multi-domain NFs in which the dipole–dipole interaction, domain wall energy and even long-range elastic energy are taken into account in addition to the Landau potential, while these interactions have less been considered in other models. In addition, this model allows us to investigate the effect of dipole defects on the ferroelectric and the dielectric properties of RFs which may not be accessible in other models. In fact, the dipole configuration and the dielectric dynamic relaxation of a mode RF system were simulated in our earlier work.[16,26–28] Here it should be mentioned that the random fluctuations imposed on the Landau potential imply a random field associated with the magnitude rather than the orientation of dipoles. Nevertheless, our preliminary simulation demonstrated that a random field directed to the orientation of dipoles does not affect much the equilibrium configuration of RFs in terms of orientation because of the role of the inter-dipole gradient energy term, while a sufficient number of orientations makes the simulation extremely tedious. We do not care much about the random field associated with dipole orientation.

In this work, we extend our simulation to the dynamic aspects of the dielectric relaxation in RFs. We focus on the study of dipole cluster feature above T_m, and the frozen superparaelectric behaviours well below T_m. Furthermore, we evaluate the time–domain distribution of the dielectric relaxations of both NFs and RFs, from which we identify the extended time-domain spectrum and consequently explain the diffusive transition behaviours of RFs.

2. Model and Monte Carlo simulation

In this section we present a brief description on the GL model of ferroelectrics with dipole defects, although it was extensively studied.[11,15,16] We investigate the T-dependent evolution of the equilibrium dipole configuration through using Monte Carlo (MC) simulation. The MC simulation is performed

on a two-dimensional (2D) $L \times L$ lattice with periodic boundary conditions, where the PE and the FE phases take the square and the rectangular configurations, respectively. For each lattice site, a dipole vector $\boldsymbol{P} = (P_x(\boldsymbol{r}),\ P_y(\boldsymbol{r}))$ where P_x and P_y are the two components along x- and y-axis, respectively, is characterized with its moment and orientation defined by the energy minimization. The lattice Hamiltonian includes the Landau double-well potential, the long-range dipole–dipole interaction and the gradient energy associated with domain walls. The long-range elastic energy will not be taken into account because this energy term is not important for RFs while its calculation is very time-cunsuming.[26−28]

The Landau double-well potential $f_{\rm L}$ takes the following form:

$$\begin{aligned} f_{\rm L}(P_i) \,=\, & A_1(P_x^2 + P_y^2) + A_{11}(P_x^4 + P_y^4) \\ & + A_{12}P_x^2P_y^2 + A_{111}(P_x^6 + P_y^6), \end{aligned} \tag{1}$$

where subscript i refers to lattice site i, A_1, A_{11}, A_{12} and A_{111} are the energy coefficients, respectively. For NFs, a non-zero dipole is favoured if $A_1 < 0$ which may take one of the four orientations: [±1, 0] and [0, ±1].

The gradient energy $f_{\rm G}$ at site i can be written as

$$\begin{aligned} f_{\rm G}(P_{i,j}) \,=\, & \frac{1}{2}G_{11}(P_{x,x}^2 + P_{y,y}^2) + G_{12}P_{x,x}P_{y,y} \\ & + \frac{1}{2}G_{44}(P_{x,y} + P_{y,x})^2 \\ & + \frac{1}{2}G'_{44}(P_{x,y} - P_{y,x})^2, \end{aligned} \tag{2}$$

where $P_{i,j} = \partial P_i/\partial x_j$, and G_{11}, G_{12}, $G_{44} = G'_{44}$ are all positive material parameters. This gradient term prefers long-range FE ordering. The dipole–dipole interaction $f_{\rm dip}$ for site i in SI units can be written as

$$f_{\rm dip}(P_i) = \frac{B}{8\pi\varepsilon_0\chi}\sum_{<j>}\left[\frac{\boldsymbol{P}(r_i)\cdot\boldsymbol{P}(r_j)}{|r_i - r_j|^3} - \frac{3\left[\boldsymbol{P}(r_i)\cdot(r_i - r_j)\right]\left[\boldsymbol{P}(r_j)\cdot(r_i - r_j)\right]}{|r_i - r_j|^5}\right], \tag{3}$$

where B is a constant, $\langle j\rangle$ represents a summation over all sites within a separation radius R centred at site i, parameters r_i, r_j, $\boldsymbol{P}(r_i)$ and $\boldsymbol{P}(r_j)$ here should be vectors, r_i and r_j are the coordinates of sites i and j, respectively. In a strict sense, R should be infinite but an effective cut-off at $R = 8$ is reliable for our simulation.[29] The electrostatic energy induced by external electric field E is

$$f_E(P_i) = -P_i \cdot E, \tag{4}$$

which takes the [1, 0] orientation. The Hamiltonian for the 2D lattice is expressed as

$$H = \sum_{\langle i\rangle} f_{\rm L} + f_{\rm G} + f_{\rm dip} + f_E. \tag{5}$$

We now extend the above GL model by introducing dipole defects. The defects are introduced into the lattice by imposing fluctuations on parameter A_1 for site i if this site is defective while the other parameters remain unchanged. One may refer to earlier reports on detailed discussion.[11,15,16] We have:

$$\begin{aligned} & A_1(r_i) = A_{10} + b_m \cdot c, \\ & A_{10} = \alpha(T - T^0), \quad \alpha > 0, \end{aligned} \tag{6}$$

where $\alpha > 0$ is a material constant, T^0 is the critical temperature for an NF crystal (usually $T^0 \leq T_{\rm c}$), c takes 0 or 1 to represent a perfect site or a defective site, $b_{\rm m}$ is the coefficient characterizing the influence of defects on T^0. We denote the defect concentration in the lattice by C_0, representing L^2C_0 defects randomly distributed in the lattice.

To illustrate the internal random field as generated by the doped defects, we take the case of $T = T^0$ as an example. For a lattice site i, $A_1(r_i) > 0$ if $b_{\rm m} > 0$, implying defect-suppressed ferroelectricity, and $A_1(r_i) < 0$ if $b_{\rm m} < 0$ for enhanced ferroelectricity. We define a second variable $C_{\rm p} \in [0, 1]$, which means $C_0 \cdot C_{\rm p} \cdot L^2$ defect sites with $b_{\rm m} > 0$ and the left $C_0 \cdot (1 - C_{\rm p}) \cdot L^2$ sites with $b_{\rm m} < 0$. The value of $b_{\rm m}$ for a site is randomly taken from a range $[0, 1]b_{\rm M}$ for $b_{\rm m} > 0$ and $[-1, 0]b_{\rm M}$ for $b_{\rm m} < 0$, where $b_{\rm M} > 0$ scales the strength of the random field induced by the defects.

Within the framework of Debye relaxation, the dielectric relaxation of the lattice is defined by dynamic dielectric susceptibility $\chi = \chi' + {\rm i}\,\chi''$, with[15,16]

$$\begin{aligned} \chi' &= \frac{C}{NT}\left\langle\sum_i^N \frac{1}{1 + (\omega\cdot\tau/\omega_0)^2}\right\rangle, \\ \chi'' &= \frac{C}{NT}\left\langle\sum_i^N \frac{\omega\cdot\tau/\omega_0}{1 + (\omega\cdot\tau/\omega_0)^2}\right\rangle, \end{aligned} \tag{7}$$

where $\langle\ \rangle$ represents the configuration averaging, χ' and χ'' are the real and the imaginary parts, ω is the frequency of external electric field E, ω_0 is the polariton frequency ($\omega_0 = 1$ for simplification), $N = L^2$ and C is a temperature independent constant. Here, time τ depends on both the local Landau potential and dipole flip among those candidate states at site i, which can be written as:

$$\tau = \tau_0 \cdot \tau' = \tau_{00} \exp(-f_{\rm L}/kT) \cdot \tau', \tag{8}$$

where τ_0 is the characteristic flip time for a non-interacting system, which is actually determined by the energy barrier referring to $f_{\rm L}$ in the mean-field approximation, $\tau_{00} = 1.0$ is the pre-exponential factor which scales the characteristic time for lattice vibration, and τ' is the averaged inverse number of flips for the dipole at site i per Monte Carlo step (MCS).

The detailed procedures of the simulation and the parameter choice were reported earlier.[16] Some of the material parameters are converted into the dimensionless ones as done by Hu and Chen.[30] All parameters chosen for the simulation are given in Table 1, which do not refer to any real materials, although their values are chosen by referring to the parameters of $BaTiO_3$. In our simulation, $C_{\rm p} = 0.5$ is fixed, which means that half of the dipole defects tend to enhance the local polarization, and the other half tend to suppress the local polarization. C_0 and $b_{\rm M}$ are treated as variables. In addition, field $E = E_{\rm m}\sin(2\pi\omega t)$, where $E_{\rm m}$ is the ac-signal amplitude and t is time. We take $T^0 = 4.0$ in our simulation.

Table 1. Parameters chosen for the present simulation.

T^0	4.0	α	1.0
A_{11}	–0.5	A_{12}	9.0
A_{111}	0.8	G_{11}	3.0
G_{12}	0.6	G_{44}	3.0
$b_{\rm M}$	0.0–20.0	L	64
$C_{\rm p}$	0.5	C_0	0.0–01.0

What should be mentioned here is that for a reliable simulation, a 3D lattice should be employed. However, the computational capacity is extremely big and because we do not focus much on the critical phenomena associated with the FE phase transitions, all of our simulations will be performed on a 2D lattice. We once employed a 16×16×16 cubic lattice for a presimulation and did not find significant difference of the simulated results (e.g. dielectric relaxation) from those we obtained for a 2D lattice of $L \sim 64$. Furthermore, a quantitative comparison of the simulation results with experimental results on $BaTiO_3$ is not available since in one hand no many dielectric data on doped $BaTiO_3$ are available, and on the other hand we take into account neither the lattice symmetry nor long-range elastic energy of $BaTiO_3$.

3. Results of simulation and discussion

3.1. Dipole configuration

We first investigate the 2D dipole configurations at different values of T for RFs, and the snapshoted images at $T = 5.2$, 4.2 and 2.0, respectively, for an RF lattice of $C_0 = 1.0$ and $b_{\rm M} = 5.0$, are shown in Figs. 1(a)–1(c) (left column). For comparison, we also present the snapshoted images for a NF ($C_0 = 0.0$) in Figs. 1(d)–1(f) (right column).

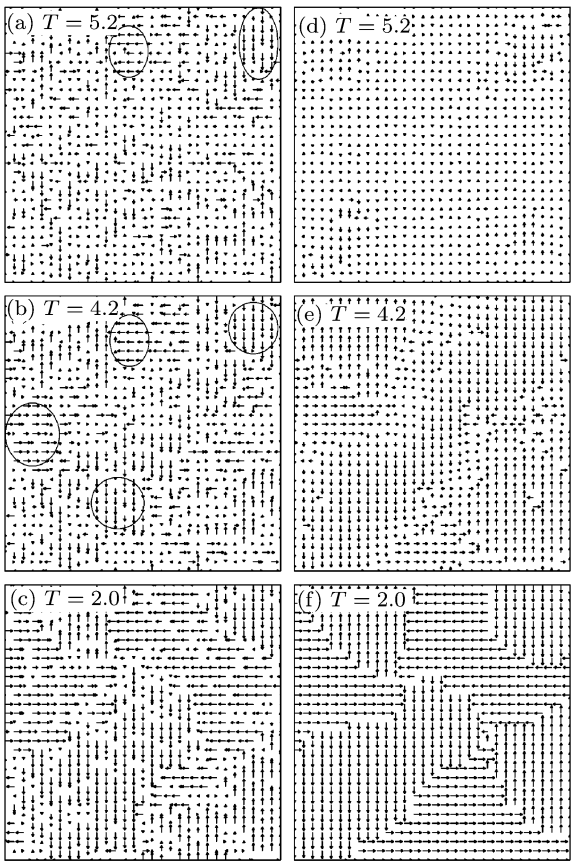


Fig. 1. Snapshoted dipole configurations for an RF lattice (left column, $C_0 = 1.0$, $b_{\rm M} = 15$) and an NF lattice (right column) at several temperatures as indicated. $T^0 = 4.0$. The open circles cover the FE nano-clusters.

It is clearly shown that at $T = 5.2 > T^0$, one already observes dipole clusters in the RF lattice as

indicated by open circles in Fig.1(a), although these dipole clusters are very small in size and well isolated from one and another. They are randomly oriented along one of the four orientations and no spatial correlation between them can be identified although the energetic inter-cluster interactions cannot be excluded. However, at this temperature the lattice in Fig. 1(d) shows homogeneous PE phase, indicating typical NF features above T_c.

As $T = 4.2$, very close to $T^0 = 4.0$ as shown in Fig. 1(b), much more dipole clusters appear in the lattice and their sizes are also larger than those shown in Fig. 1(a). The lattice exhibits typical structure of RFs with coexisting dipole clusters (or more polarized regions) and PE matrix (or less polarized regions). At this temperature, the lattice transits from PE state into typical NF state and the dipole alignment for NF (Fig. 1(e)) is already long-ranged. As $T = 2.0 << T^0$, the dipole clusters in the RF lattice continue growing, and significant inter-cluster coalescence occurs and eventually forms long-range order dipole configuration as shown in Fig. 1(c), whereas Fig. 1(f) shows a typical multi-domained NF structure. A comparison between Fig. 1(c) and Fig. 1(f) allows us to argue that the RF lattice may begin to frustrate at $T < 2.0$ and the dipole configuration is quite similar to the multi-domained structure of NFs, although there are still high dipole defects inside the domains. In fact, because we only employ the Debye mechanism of dielectric relaxation to evaluate the dielectric susceptibility as shown below, the frozen temperature for RFs would be close to $T = 0$.

The above simulated dipole configurations at different values of T seem to reveal the main features of RFs, suggesting that the defect model as an approach to RFs is physically sound. We then further investigate the dynamic dielectric susceptibility as a function of T and dipole defects.

3.2. Dielectric susceptibility

We calculate the values of dielectric susceptibility (χ' and χ'') as a function of T for a set of lattices with different values of C_0 and b_M. As an example, we present in Figs. 2(a) and 2(b) the simulated results for $C_0 = 1.0$ and $\omega = 0.05$ mcs^{-1} but with b_M from 0.0 to 15.0. Here mcs (Monte Carlo step) is a time unit in Monte Carlo simulation. As $b_M = 0.0$, corresponding to the NF lattice, χ' and χ'' as functions of T mark the typical ferroelectric phase transitions at $T \approx 4.2$, featured by the sharp transition peaks. When b_M increases up to $b_M = 6.0$, the transition peak becomes significantly broadening, while the peak position remains roughly unchanged. Further increasing of b_M from 6.0 to 15.0 seems to result in the behaviours of superparaelectric relaxation, characterized by the tremendous rising of χ' in the low-T regime below T_c, while $\chi'(T)$ at $T \approx T_c$ shows a broad saddleback feature. In particular, at $b_M = 15.0$, the low-T susceptibility exhibits the exponential growth with T decreasing, a typical feature of low-T superparaelectric behaviour, which is to be discussed below.

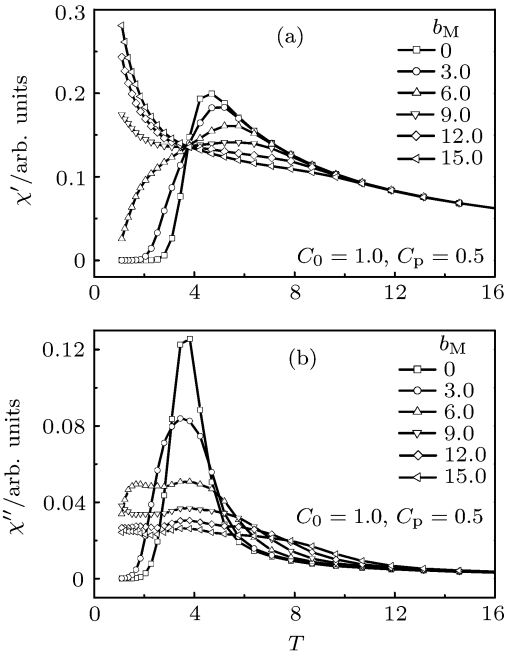


Fig. 2. Real part $\chi' - T$ (a) and imaginary part $\chi'' - \log(T)$ of simulated dielectric susceptibility for various values of b_M, $C_0 = 1.0$, $E_m = 30.0$ and $\omega = 0.05$ mcs^{-1}.

Corresponding to $\chi'(T)$, $\chi''(T)$ shows a sharp peak at the low-T front of $\chi'(T)$ peak for NFs and the sharp peak becomes gradually diffusive with b_M increasing until the broad plateau as b_M increases up to 9.0 and above. The simulated behaviours are essentially the same as those observed for RFs.

3.3. Dipole cluster states

The broad transition profile of $\chi'(T)$ around the transition peak for RFs is an indication of dipole cluster state above T_m. To illustrate this phenomenon, we replot the curves for $1/\chi'$ as a function of T above T_m for a series of RFs with $C_0 = 1.0$ and $b_M = 0.0$ to 15.0 in Fig. 3(a). For $b_M = 0.0$, i.e. an NF lattice, $1/\chi'(T)$ shows a linear dependence of T above T_m, according to the Curie–Weiss law, as demonstrated here. We

present as an inset the locally amplified dipole configuration for this lattice at $T = 5.2 > T_c \sim 5.0$, which shows homogeneous PE state. As $b_M > 0$, we observe a clear positive deviation of $1/\chi'(T)$ from the linear dependence. The bigger the value of b_M is, the more serious the positive deviation will be. Correspondingly, we present as insets the locally amplified dipole configurations of these RFs at $T = 5.2$, 5.6, 6.6, 8.1 and 9.2 for $b_M = 3.0$, 6.0, 9.0, 12.0 and 15.0, respectively. Dipole clusters are identified for each case, as labeled by open circles, although the temperatures at which these dipole configurations are snapshoted are well above T_m. As $b_M = 15.0$, ordered dipole clusters can be identified even at $T = 9.2 >> T_m$, although these clusters are well separated from each other and small in size. These results indicate that for RFs the ordered dipole cluster state is already stable at a temperature well above T_m.

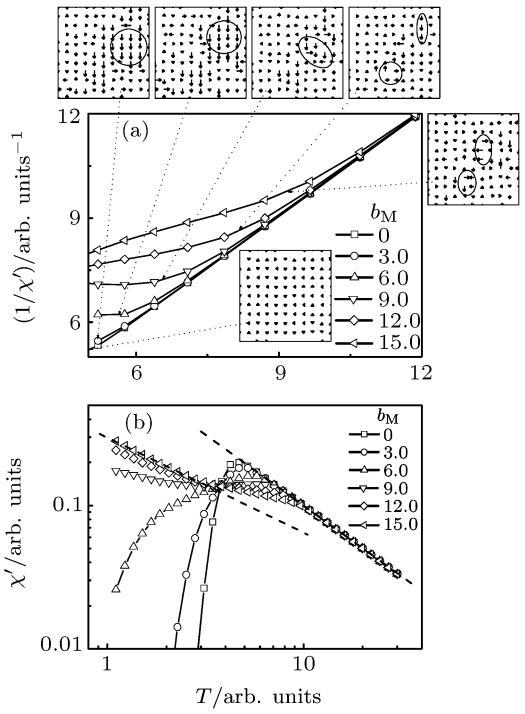


Fig. 3. (a) Curves for simulated $1/\chi'$ as a function of T for various values of b_M, where insets show the locally amplified dipole configurations corresponding to various $1/\chi' - T$ curves at various temperatures, and (b) simulated $\log(\chi') - \log(T)$ curves with $C_0 = 1.0$, $E_m = 30.0$ and $\omega = 0.05$ mcs^{-1}.

To evaluate the temperature dependence of the statistically averaged dipole cluster size, one may consult the concept of Griffiths phase which is widely employed to describe the spin cluster states above the Curie point for inhomogeneous magnetic systems.[31,32] The concept of Griffiths phase is based on percolation effects in diluted magnets with the nearest neighbouring interaction, and it relies on the finite probability of finding sufficiently large clusters of magnetic species interacting with other magnetic species. The physical problem studied here is conceptually different from the above. However, here we take only the form with the Griffiths phase to roughly illustrate the dipole cluster state of RFs. If a similar phase (not in physical essence) can be defined for the dipole cluster phase in RFs, we may assume that each dipole in dipole clusters has a constant moment $p = 1$ within the finite temperature regime above T_m, although this assumption is not physically sound. Then, we have

$$1/\chi' \propto \frac{T_m}{P+1}\left(\frac{T}{T_m} - 1\right), \tag{9}$$

where $(P + 1)$ is the effective dipole moment of the dipole clusters. For NFs, $P = 0$ because no dipole cluster exists in the lattice and Eq. (9) recovers back to the Curie–Weiss law. From Eq. (9) one sees that the local slope of $1/\chi'$ as a function of T is proportional to $(P + 1)^{-1}$, indicating the smaller the slope is, the larger the value of P will be. Therefore, one understands from Fig. 3(a) that the dipole cluster size increases with T decreasing and b_M increasing, respectively, demonstrating the dipole cluster state of RFs above T_m.

In Fig. 3(b) we plot the simulated $\chi' - T$ relationships in the $\log - \log$ coordinates for the RFs with $b_M = 0.0$ to 15.0, in order to investigate the superparaelectric behaviours at low-T regime. Over the high-T regime, the perfect linear $\log\chi' - \log T$ relation is shown for all the cases as long as $T >> T_m$, typical paraelectric behaviour. Over the low-T regime well below T_m, we also observe the linear relationship between $\log\chi'$ and $\log T$ as long as b_M is large enough, indicating the possible superparaelectric behaviour of the RFs. In fact, take the cases of $b_M > 6.0$ as examples, the slopes of the $\log\chi' - \log T$ lines over the low-T regime are much smaller than those of the high-T $\log\chi' - \log T$ lines, indicating that the sizes of the dipole clusters in the low-T regime is larger than in the high-T regime. The larges the size is, the smaller the value of b_M will be. Looking back to Fig. 1(c), the dipole configuration at T=2.0, one understands that the dipole clusters at low-T keep close to each other, thus strong inter-cluster interaction can be expected. These clusters may be eventually frozen when T decreases further. All of these results support the low-T superparaelectric state of RF lattice studied here.

3.4. Dielectric dispersion and Vogel–Fulcher relation

The dipole cluster state of RFs as revealed above can be further characterized by the frequency dispersion of the $\chi' - T$ dependence. The underlying physics is that these clusters may have their own characteristic time of relaxation, which is dependent on cluster size, although the inter-cluster interactions may more or less modulate these characteristic times. As an example, we show in Fig. 4(a) the evaluated $\chi' - T$ relationships for the RF with $C_0 = 1.0$ and $b_{\rm M} = 5.0$ under different frequencies. The arrow indicates the increasing of frequency ω. As expected, the $\chi' - T$ relation does exhibit remarkable frequency dispersion, characterized by the significant down-right shifting of the transition peak increasing ω.

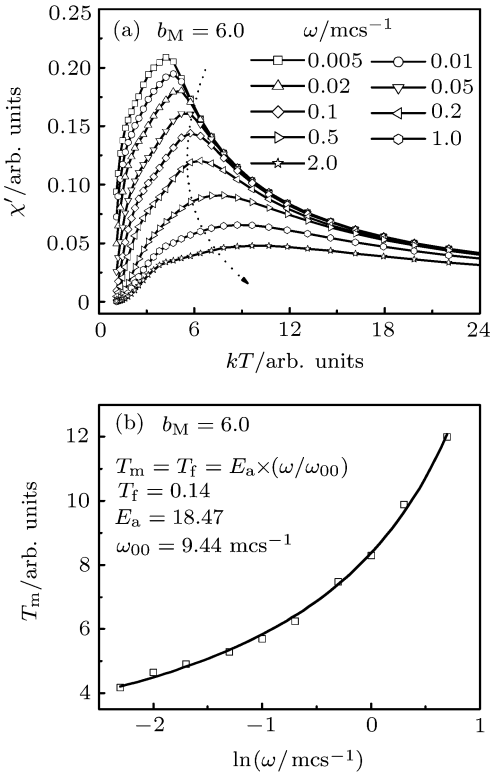


Fig. 4. (a) Curves for simulated χ' as a function of T at different values of frequency ω, and (b) evaluated $T_{\rm m}$ as a function of frequency ω, with $C_0 = 1.0$, $b_{\rm M} = 6.0$ and $E_{\rm m} = 30.0$.

Furthermore, the significant frequency dispersion effect shown in Fig. 4(a) allows one to check the applicability of the Vogel–Fulcher relation which is usually thought to hold for RFs. This relation reads[4]

$$\omega = \omega_{00} \cdot \exp\left(-\frac{E_{\rm a}}{(T_{\rm m} - T_{\rm f})}\right), \qquad (10)$$

where ω_{00} is the pre-exponential factor, $E_{\rm a}$ the thermal-activation energy for the dipole clusters, and $T_{\rm f}$ the frozen point below which the clusters are essentially frozen and the thermally driven relaxation becomes negligible.

As mentioned above, we evaluate the dielectric susceptibility according to the Debye mechanism only, which means that for the present model, $T_{\rm f}$ would be close to zero. Under this assumption, we plot $T_{\rm m}$ as a function of $\log(\omega)$ in Fig. 4(b). A good fitting of the simulated data by Eq. (10) is given, indicating the applicability of the Vogel–Fulcher relation. Secondly, $E_{\rm a} = 17.20$ is much bigger than $(f_{\rm LD} + f_{\rm dip} + f_{\rm G})$ for a dipole in the NF lattice, reflecting that the relaxation is for dipole cluster rather than a single dipole. These results thus support the argument that dipole cluster state is favoured in RFs.

3.5. Time-domain distributions of dielectric relaxation

The broad temperature regime of the FE transitions for RFs allows one to speculate that the time-domain distribution of the dielectric relaxation is very broad. To check this speculation, we may evaluate the time-domain distribution $G(\log\tau, T)$ by the following approach:[8]

$$\int_0^\infty G(\log\tau, T) \cdot {\rm d}(\log\tau) = 1,$$

$$\chi'(\omega, T) = \chi'_{\rm s} \int_0^\infty G(\log\tau, T) \cdot {\rm d}(\log\tau), \qquad (11)$$

where τ is the relaxation time, and $\chi'_{\rm s}$ is the static susceptibility. However, in the present work this distribution can be evaluated directly from Eq. (8) and the simulated data.[33]

The evaluated $G(\log\tau, T)$ at $T = 7.2$, 4.7 and 3.0 for the NF lattice ($b_{\rm M} = 0.0$) and two RFs with $b_{\rm M} = 6.0$ and 12.0, are presented in Figs. 5(a)–5(c), respectively. Here, $E_{\rm m} = 15$ and $\omega = 0.005$ mcs^{-1}. From Fig. 5, one observes that for the NF lattice, distribution $G(\log\tau, T)$ at each temperature is single-peaked. At the PE state ($T = 7.2$), the peak profile is very sharp. Upon T decreasing from the PE state into the FE states ($T = 4.7$ and 3.0), $G(\log\tau, T)$ becomes significantly broadened in the absolute time scale, and the peak position shifts considerably towards the long-time domain. These features are typical of NFs where the dipole relaxation is believed to occur rapidly in a

cooperative manner due to the long-range dipole ordering.

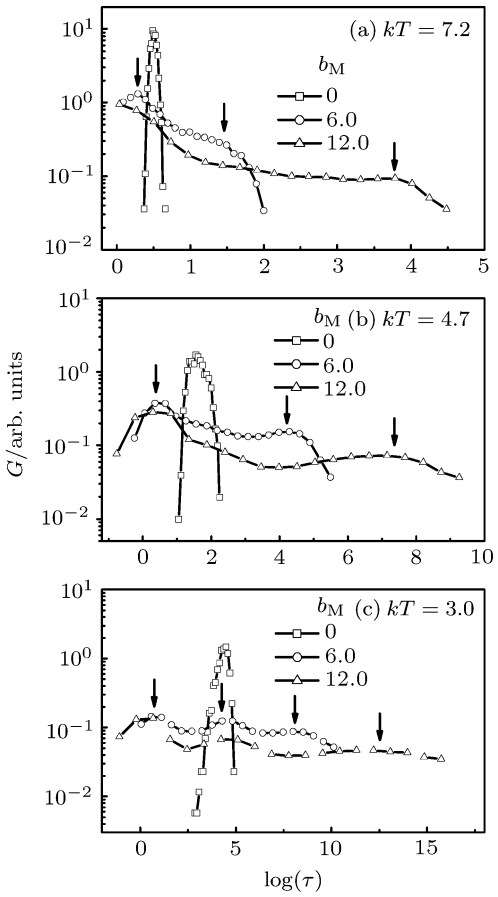


Fig. 5. Simulated time-domain distributions of the dielectric relaxation for an NF lattice ($b_M = 0$) and two RF lattices ($b_M = 6.0$ and 12.0) at $T = 7.2$ (a), 4.7 (b), 3.0 (c), with $C_0 = 1.0$, $E_m = 30.0$ and $\omega = 0.05$ mcs^{-1}.

However, the evaluated distributions for RFs show very different behaviours. At $T = 7.2$ in the PE state, $G(\log\tau)$ is single-peaked, but the peak profile is much broader than that of the NF lattice. The bigger the value of b_M is, the broader the distribution will be. More interestingly, it is observed that $G(\log\tau)$ shows a clear saddle-back shoulder in the long time tail if plotted in a logarithmic scale, which is indicated by arrows in Fig. 5(a). This is an imprint that $G(\log\tau)$ at a given temperature may no longer be single-peaked. In fact, as T goes down to $T = 4.7 \sim T_m$, for the two RF lattices ($b_M = 6.0$ and 12.0), the peaks of $G(\log\tau)$ are not only very broad but also exhibit broad double-peaked patterns. The left peak corresponds to a time shorter than that for the NF lattice and the right peak to a time much longer than that for the NF lattice. If T is further reduced down to $T = 3.0$ in the deep RF regime, the curves of $G(\log\tau)$ of the two RFs become multi-peaked, as indicated by the arrows shown in Fig. 5(c).

To understand the multi-peaked distributions of the relaxation times, we may consult to the dipole cluster state of RFs. In fact, the dynamic responses of RFs to external fluctuations are different from those of NFs where the long-range FE ordering does not allow sufficient relaxation of local dipoles alone due to the inter-dipole interaction unless the relaxation is in the cooperative manner. The dipole clusters in RFs may respond to external fluctuations either by local dipole re-orientation or through a spatial shift from their equilibrium positions, or by both.[6] If each dipole is treated as a relaxator and no interaction between these relaxators is considered, RF usually offers a very broad monotonic or single-peaked distribution of relaxation time, thus resulting in diffusive phase transition and remarkable frequency dependence of the dielectric relaxation. However, one has a reason to argue that the dipoles inside one dipole-cluster are not independent of each other, but they are interactive. Therefore, all dipoles inside a cluster relax in a cooperative manner. In a rough sense, the dipole clusters and the PE matrix phase have their own time distributions and characteristic times (peaked times) of dielectric relaxation, respectively. Because of the different types of dipole defects and sizes of the clusters, the evaluated distribution represents a superposition of the individual monotonic or single-peaked distributions. If the peaks of these distributions are well separated from each other in the time-domain, a double-peaked or multi-peaked pattern becomes inevitable. Surely, if the random field intensity (b_M) due to the defect doping is not so strong enough that these peaks are separated far from each other, a simple superposition of them may develop into a broad (diffusive) single-peaked distribution. When b_M is large enough ($b_M > 6.0$), the multi-peaked pattern is the natural outcome.

Unfortunately, up to date we have no direct experimental evidence for the multi-peaked time distribution of the dielectric relaxation. Experimentally, $G(\log\tau, T)$ is derived by Eq. (11) from experimental $\chi' - T$ data at different frequencies. However, due to the limited ω-range covered, the time domain covered by $G(\log\tau, T)$ is limited too. Furthermore, for those RFs often studied, like $Pb(Mg_{1/3}Nb_{2/3})O_3$, Zr(Hf)-doped $BaTiO_3$ and La(Pr)-doped $Pb(Zr,Ti)O_3$, the diffusive phase transitions occur at relatively high temperatures.[34,35] The thermal flip times for dipoles

or dipole clusters between normal FE and RFE may not be very different in the sense of order of magnitude, which does not allow the reliable checking of the multi-peaked distribution. Nevertheless, it would be possible to check this predicted effect if an RFE of phase transition point as low as 100K or even lower can develop, in which the relaxation time scale may be as broad as more than 10–20 orders of magnitude. For such cases, we expect a multi-peaked time-domain distribution of the dielectric relaxation.

4. Conclusion

We present a Monte Carlo simulation on the dipole configuration and dielectric relaxation of RFs by using the Ginzburg–Landau theory of ferroelectrics with random field induced by dipole defects. We successfully reproduce the dipole microstructures of RFs where dipole clusters are embedded in the PE matrix. The evaluated dielectric susceptibility and its frequency dispersion demonstrate the dipole cluster state in the high temperature regime above the ferroelectric transitions and the superparaelectric behaviour at low temperature regime below the ferroelectric transitions. The time-domain distribution of the dielectric relaxation below the ferroelectric transitions exhibits the multi-peaked pattern with multi-characteristic times instead of monotonic or diffusive single-peaked pattern. The present dipole defect model reproduces all of the main features of RFs, demonstrating the applicability of the dipole defect model as a good approach to RFs.

References

[1] Pirc P and Blinc R 1999 *Phys. Rev.* B **60** 13470
[2] Blinc R, Laguta V and Zalar B 2003 *Phys. Rev. Lett.* **91** 247601
[3] Vakhrushev S B and Shapiro S M 2004 *Phys. Rev.* B **70** 134110
[4] Glazounov A E and Tagantsev A K 2000 *Phys. Rev. Lett.* **85** 2192
[5] Kingon A I, Streiffier S K, Basceri C and Summerfelt S R 1996 *MRS Bull.* **21** 46
[6] Settler N and Cross L E 1980 *J. Appl. Phys.* **51** 4356
[7] Cross L E 1987 *Ferroelectrics* **76** 241
[8] Tyunina M and Levoska J 2005 *Phys. Rev.* B **72** 104112
[9] Vugmeister B E and Glinchuk M D 1990 *Rev. Mod. Phys.* **62** 993
[10] Yao X, Chen Z and Cross L E 1983 *J. Appl. Phys.* **54** 3399
[11] Semenovskaya S and Khachaturyan A G 1998 *J. Appl. Phys.* **83** 5125
[12] Zhang Q M. Zhao J, Shrout T R and Cross L E 1997 *J. Mater. Res.* **12** 1777
[13] Park C H and Chadi D J 1998 *Phys. Rev.* B **57** 13961
[14] Wu Z, Duan W, Wang Y, Gu B L and Zhang X W 2003 *Phys. Rev.* B **67** 052101
[15] Su C C, Vugmeister B and Khachaturyan A G 2001 *J. Appl. Phys.* **90** 6345
[16] Liu J M, Wang X, Chan H L W and Choy C L 2004 *Phys. Rev.* B **69** 094114
[17] Prosandeev S A, Cockayne E and Burton B P 2003 *Phys. Rev.* B **68** 014120
[18] Rytz D, Höchli U T and Bilz H 1980 *Phys. Rev.* B **22** 359
[19] Burton B P, Cockayne E and Waghmare U V 2005 *Phys. Rev.* B **72** 064113
[20] Tiwari V S, Singh N and Pandey D 1995 *J. Phys.: Condens. Matter* **7** 1441
[21] Cao W and Cross L E 1991 *Phys. Rev.* B **44** 5
[22] Nambu S and Sagala D A 1994 *Phys. Rev.* B **50** 5838
[23] Zhang Y F, Wang C L, Zhao M L, Li J C and Zhang R Z 2009 *Chin. Phys.* B **18** 1665
[24] Zhou J, Lu T Q, Xie W G, Zhou J and Cao W W 2009 *Chin. Phys.* B **18** 3054
[25] Sun P N, Cui L and Lu T Q 2009 *Chin. Phys.* B **18** 1658
[26] Wang L F and Liu J M 2006 *Appl. Phys. Lett.* **89** 092909
[27] Wang L F and Liu J M 2007 *Appl. Phys. Lett.* **90** 062905
[28] Wang L F and Liu J M 2007 *Appl. Phys. Lett.* **91** 092908
[29] Li B L, Liu X P, Fang F, Zhu J L and Liu J M 2006 *Phys. Rev.* B **73** 014107
[30] Hu H L and Chen L Q 1997 *Mater. Sci. Eng.* A **238** 182.
[31] Salamon M B, Lin P and Chun S H 2002 *Phys. Rev. Lett.* **88** 197203
[32] Wang K F, Wang Y, Wang L F, Dong S, Li D, Zhang Z D, Yu H, Li Q C and Liu J M 2006 *Phys. Rev.* B **73** 134411
[33] Liu J M, Dong S, Chan H L W and Choy C L 2006 *J. Phys.: Conden. Matter* **18** 8973
[34] Anwar S, Sagdeo P R and Lalla N P 2006 *Solid State Commun.* **138** 331
[35] Lu Z G and Calvarin G 1995 *Phys. Rev.* B **51** 2694